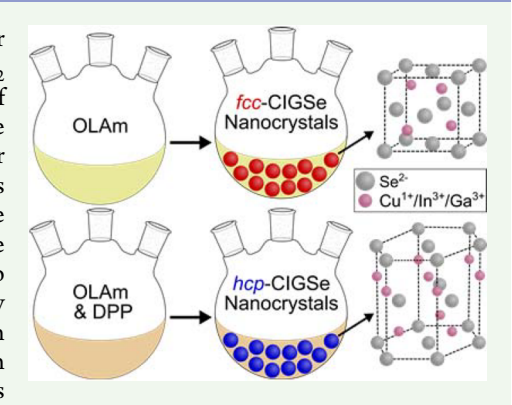
CuGaSe₂ and CuIn_xGa_{1-x}Se₂ Nanocrystals with Sphalerite or Wurtzite **Phase for Optoelectronic Applications**

Daniel W. Houck, Simmi V. Nandu, Timothy D. Siegler, and Brian A. Korgel*

McKetta Department of Chemical Engineering and Texas Materials Institute, The University of Texas at Austin, Austin, Texas 78712, United States

Supporting Information

ABSTRACT: There has been significant interest in I-III-VI2 nanocrystals for photonic and optoelectronic applications, especially solar cells. CuInSe2 nanocrystals have been studied extensively as model materials for this class of compounds. By incorporation of Ga to make CuIn, Ga_{1-x}Se₂ (CIGSe), the optical gap can be tuned by composition as well as size for higher efficiency solar cells or other applications. The synthesis of CIGSe nanocrystals, however, has not been studied in much detail. It turns out that the addition of Ga to the typical arrested precipitation reactions for CuInSe₂ nanocrystals in oleylamine (OLAm) leads to very slow particle nucleation and growth rates. In order to achieve consistent morphology, reaction yield, and Ga incorporation, a lengthy (~24 h) low temperature incubation step is needed. Under these slow growth conditions, the crystal structure of the CIGSe nanocrystals is cubic. By addition of diphenylphosphine (DPP) to the reactions, the nucleation and growth rates



are significantly increased; however, this leads to CIGSe (and CuGaSe₂) nanocrystals with wurtzite phase. In contrast, CuInSe₂ nanocrystals made under similar fast-growth conditions are always cubic.

KEYWORDS: X-ray diffraction, copper indium gallium selenide nanocrystals, arrested precipitation, nanocrystal growth kinetics, metastable phase

INTRODUCTION

Downloaded via UNIV OF TEXAS AT AUSTIN on March 16, 2020 at 17:42:46 (UTC). See https://pubs.acs.org/sharingguidelines for options on how to legitimately share published articles.

Colloidal nanocrystals of I-III-VI2 compounds are being developed for a number of applications, including photovoltaic devices (PVs), luminescent solar concentrators, and fluorescence imaging contrast agents.^{1–7} Copper indium gallium diselenide (CuIn_xGa_{1-x}Se₂, CIGSe) nanocrystals are especially interesting for PVs, due in part to the fact that bulk, polycrystalline CIGSe films can provide very high power conversion efficiency on both glass and flexible substrates. 8-13 CIGSe nanocrystals can be deposited from solvent-based inks and sintered by high temperature selenization to achieve polycrystalline films with relatively high efficiencies, up to nearly 14%. 10-12 Compared to CuInSe₂, CIGSe nanocrystals have an optical gap that is better suited for PVs (closer to 1.3-1.4 eV) and the presence of Ga in the CIGSe nanocrystals generally improves the quality of the films generated by high temperature selenization.¹² Here, we examine the effect of Ga in the synthesis of CIGSe nanocrystals.

The synthesis of CuInSe₂ nanocrystals is relatively wellestablished, 14-23 and Ga has been incorporated into I-III-VI₂ nanocrystals. 12,24,25 However, there has been little discussion in the literature about how Ga affects nanocrystal growth of I-III-VI2 materials. The most common way to synthesize CuInSe₂ and CIGSe₂ nanocrystals is by high temperature arrested precipitation in oleylamine (OLAm). We have found that the addition of Ga significantly slows the nucleation and growth kinetics of the nanocrystals, and in fact, Ga does not readily incorporate into CuInSe₂ nanocrystals under a range of standard growth conditions.

To overcome this, we developed a two-step arrested precipitation reaction in OLAm to synthesize CIGSe2 nanocrystals that includes a low temperature (110 °C) nucleation stage lasting ~24 h followed by a growth step at higher temperature (240 °C). This reliably produces CuIn_rGa_{1-r}Se₂ nanocrystals with desired stoichiometry, crystallinity, and relatively uniform spherical shape. Without sufficient time for nucleation in the incubation period, the nanocrystals end up with a flower-like morphology, composed of aggregated CuInSe₂ platelets that do not have Ga. The rate of CIGSe₂ nanocrystal nucleation could be significantly increased by adding diphenylphosphine (DPP). DPP is known to increase reaction rates and product yields for a variety of other nanocrystals, including CuInSe2, PbSe, and CdSe. 15,16,26-29 However, we observed that the addition of DPP also changes the resulting crystal structure of CIGSe (and CuGaSe₂) nanocrystals from cubic to hexagonal. In this case, fast nucleation and growth lead to the metastable wurtzite phase. In comparison, similar reaction conditions with fast nucleation using DPP of CuInSe₂ nanocrystals still produce nanocrystals with cubic crystal structure.

Received: June 30, 2019 Accepted: July 2, 2019 Published: July 2, 2019



■ EXPERIMENTAL SECTION

Materials. Indium(III) chloride (InCl₃, 99.99%), gallium(III) chloride (GaCl₃ 99.99%), selenium powder (Se, 99.99%), anhydrous toluene (99.8%), oleylamine (OLAm, ≥98%), and diphenylphosphine (DPP, 98%) were obtained from Sigma-Aldrich. Copper(I) chloride (CuCl, 99.999%) was obtained from Strem Chemicals. Toluene and ethanol were obtained from Fisher Scientific. OLAm was degassed by maintaining vacuum under 200 mTorr for 4 h at 110 °C and stored in a nitrogen filled glovebox. All other chemicals were used as received.

Nanocrystal Synthesis. In a three-neck 100 mL flask attached to a Schlenk line, 5 mmol (0.49 g) of CuCl and 10 mmol (0.78 mg) of Se were combined with 50 mL (152 mmol) of OLAm. Depending on the desired nanocrystals, either 5 mmol (1.11 mg) of InCl₃ was added to make CuInSe₂, 2.5 mmol (0.55 g) of InCl₃ and 2.5 mmol (0.44 mg) of GaCl₃ were added for CuIn_{0.6}Ga_{0.4}Se₂, or 5 mmol (0.88 mg) of GaCl₃ was added for CuGaSe₂. The reaction mixture was heated to 110 °C and placed under vacuum for 1 h and then blanketed with nitrogen for 24 h. The initially turbid, black reaction solution gradually becomes optically clear as nanocrystal nucleation takes place. For reactions with DPP, 1.5 mL (8.62 mmol) of DPP was added after the temperature reaches 110 °C. After 12 h, the temperature was raised to 240 °C. The heating mantle was removed after 1 h, and the reaction mixture was allowed to cool before purification.

Once the reaction mixture reached about 50 $^{\circ}$ C, 20 mL of ethanol was added and the mixture was centrifuged at 2600 rcf for 5 min. The supernatant was discarded. The precipitate was redispersed with 10 mL of toluene and centrifuged at 2600 rcf for 5 min to remove poorly capped nanocrystals. After transfer of the supernatant to another centrifuge tube, the nanocrystals were precipitated again with 5 mL of ethanol and centrifuged at 2600 rcf for 5 min. The supernatant was discarded. The nanocrystals were dispersed again in 5 mL of toluene and centrifuged at 2600 rcf to separate the remaining poorly capped nanocrystals. The supernatant was collected and then dried on a rotary evaporator to measure the mass of purified nanocrystal product. The dried powder was then moved into a N_2 -filled glovebox, dispersed in anhydrous toluene to a concentration of 100 mg/mL, and stored. It retains its colloidal stability for months.

Reactions in OLAm yielded 440 mg of dispersible CuInSe $_2$ nanocrystals (25% conversion), 750 mg of dispersible CuIn $_{0.6}$ Ga $_{0.4}$ Se $_2$ nanocrystals (45% conversion), and 520 mg of dispersible CuGaSe $_2$ nanocrystals (35% conversion). The reactions with DPP yielded 1.1 g of dispersible CuInSe $_2$ nanocrystals (60% conversion), 950 mg of dispersible CuIn $_{0.6}$ Ga $_{0.4}$ Se $_2$ nanocrystals (60% conversion), and 700 mg of dispersible CuGaSe $_2$ nanocrystals (48% conversion).

Reactions were also carried out to follow the growth process. In these cases, amounts of 10 mL were withdrawn from the reaction solution 30 min, 12 h, and 24 h after the temperature reached 110 °C. Nanocrystals were isolated from the crude reaction mixture in OLAm by precipitation with 20 mL of ethanol, followed by centrifugation at 2600 rcf for 5 min. After the supernatant was discarded, the precipitate was dispersed in 2 mL of anhydrous toluene in a nitrogenfilled glovebox. The nanocrystals left in the reaction solution after 24 h were also purified by precipitative isolation.

Materials Characterization. Powder X-ray diffraction (XRD) was performed using a Rigaku R-axis Spider diffractometer operated at 40 kV and 40 mA with Cu K α (λ = 1.54 Å) radiation. A dried powder of nanocrystals was placed on a 0.5 mm nylon loop and scanned for 10 min while rotating at 2 deg s⁻¹. Diffraction data were collected on an image plate detector and radially integrated with the Rigaku 2DP powder processing program and MDI Jade for background correction and analysis.

Transmission electron microscopy (TEM) images were obtained with an FEI Tecnai Spirit Bio Twin TEM operated at 80 kV accelerating voltage. Dilute nanocrystal dispersions in toluene (~0.125 mg/mL) were drop-cast onto TEM grids (carbon film on 200-mesh nickel grids acquired from Electron Microscopy Sciences) for imaging.

Energy-dispersive X-ray spectroscopy (EDS) measurements were carried out on a Hitachi S5500 scanning electron microscope (SEM) operated at 30 kV accelerating voltage and $10\,000\times$ magnification. Samples were prepared by drop-casting concentrated dispersions in toluene (100 mg/mL) onto a conductive boron-doped silicon wafer. Bruker Esprit software was used to fit the Cu K α , In L α , Ga K α , and Se L α emission lines to provide composition estimates.

UV-vis-NIR absorbance spectra were measured using a Cary 5000 UV-vis-NIR spectrophotometer. Nanocrystals were dispersed in toluene at a concentration of 0.1 mg/mL. Spectra were acquired with samples in quartz cuvettes with 1 cm path length.

RESULTS

Importance of a Low Temperature Nucleation Step in the Synthesis of CulnSe₂, CuGaSe₂, and ClGSe Nanocrystals in OLAm. Figure 1 illustrates the two approaches reported here to make CIGSe nanocrystals. The first involves the standard high temperature arrested precipitation of CuInSe₂ and CIGSe in OLAm. The second approach utilizes the addition of DPP to speed nucleation and growth of the nanocrystals. The typical approach of arrested precipitation in OLAm at elevated temperature required a long nucleation or an incubation period at low temperature to obtain nanocrystals that were spherically shaped and had Ga.

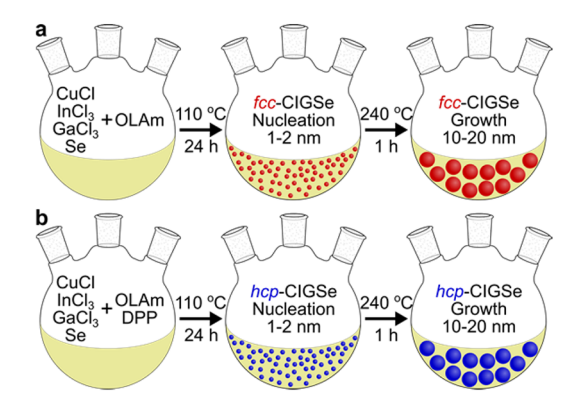


Figure 1. CIGSe nanocrystals were synthesized by two routes. (a) Nanocrystals synthesized by arrested precipitation in OLAm required a long nucleation step at 110 °C to obtain nanocrystals with Ga incorporated. Without the long nucleation step, only CuInSe₂ nanocrystals (without Ga) with a flower-like morphology were produced. (b) When DPP was added to the OLAm mixture during the nucleation step, CIGSe nanocrystals could be produced with only a brief low temperature nucleation step. DPP significantly enhanced nanocrystal nucleation. The resulting nanocrystals ended up with hcp (wurtzite) crystal structure. CuInSe₂ nanocrystals produced with the addition of DPP still had cubic crystal structure.

Figure 2 shows the TEM, XRD, and UV—vis—NIR absorbance spectra of CuInSe₂, CuIn_{0.6}Ga_{0.4}Se₂, and CuGaSe₂ nanocrystals synthesized in OLAm using such a two-step heat-up method (Figure 1a). The reaction mixture of metal chlorides and Se in OLAm is first held at 110 °C under N₂ for 24 h to provide time for nanocrystal nucleation to begin. The reaction temperature is then increased to 240 °C. By use of this process, nanocrystals are obtained that are relatively spherical and uniform in size. Although not perfect spheres, their morphology is dramatically different when made without the extended low temperature incubation. As shown in Figure 3a, the CuInSe₂ nanocrystals made with a brief incubation period of 1 h at 110 °C end up with a flower-type morphology, composed of aggregated nanoplatelets. As shown in Figure 3b for comparison, the

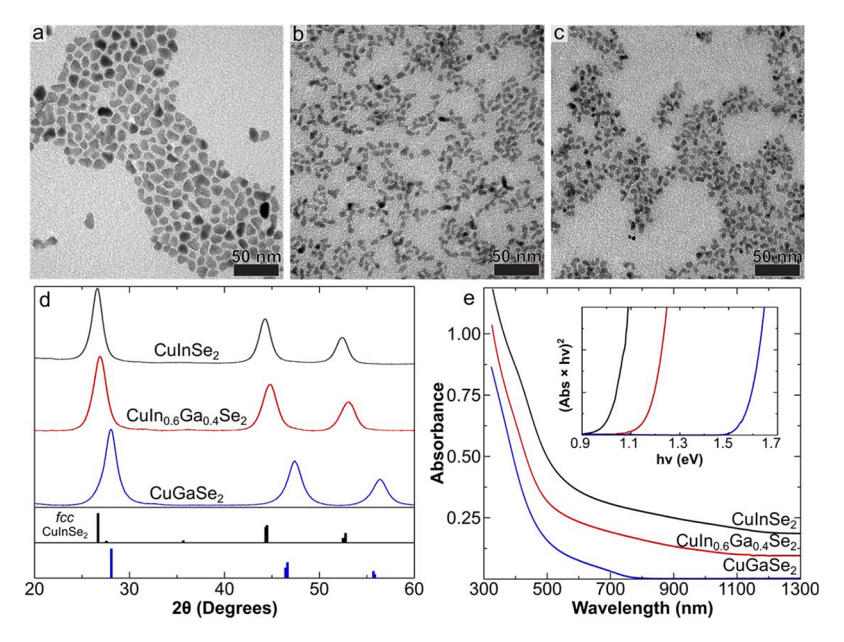


Figure 2. TEM images of (a) CuInSe₂ (b) CuIn_{0.6}Ga_{0.4}Se₂, and (c) CuGaSe₂ nanocrystals synthesized in OLAm. (d) XRD of CuInSe₂ (black), CuIn_{0.6}Ga_{0.4}Se₂ (red), and CuGaSe₂ (blue) nanocrystals and reference patterns for fcc CuInSe₂ (JCPDS no. 00-040-1487) and CuGaSe₂ (JCPDS no. 00-035-1100). (e) Room temperature UV-vis-NIR absorbance spectra of CuInSe₂ (black), CuIn_{0.6}Ga_{0.4}Se₂ (red), and CuGaSe₂ (blue) nanocrystals dispersed in toluene. The spectra are vertically offset for clarity. Inset: Plot of (Abs $\times h\nu$)² vs $h\nu$ used to estimate the optical gaps of the nanocrystals of 1.01 eV, 1.18 eV, and 1.58 eV for CuInSe₂, CuIn_{0.6}Ga_{0.4}Se₂, and CuGaSe₂, respectively.

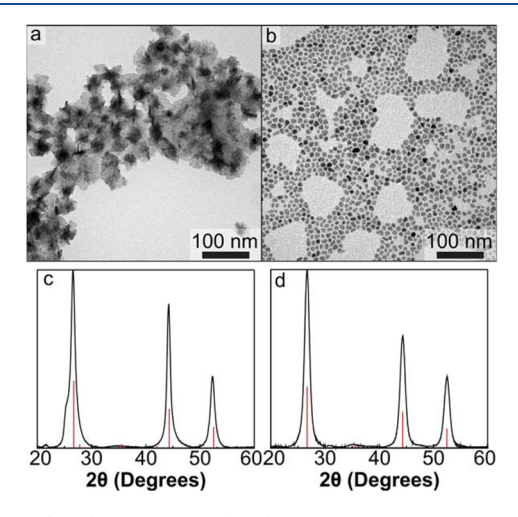


Figure 3. (a, b) TEM and (c, d) XRD of CuInSe₂ nanocrystals synthesized in OLAm using the two-step heat-up method illustrated in Figure 1 with different low temperature incubation times. The data in (a) and (c) correspond to nanocrystals made with a relatively brief low temperature incubation at 110 °C for 4 h before heating at 240 °C for 1 h. These nanocrystals have a flower-like morphology with cubic crystal structure. The data in (b) and (d) correspond to nanocrystals made with a longer low temperature incubation at 110 °C for 12 h and then heating at 240 °C for 1 h. These nanocrystals are relatively spherical with cubic crystal structure. The red lines in (c) and (d) correspond to the diffraction pattern for fcc CuInSe₂ (JCPDS no. 00-040-1487).

CuInSe₂ nanocrystals made with the low temperature extended incubation period are nearly spherical in shape. The incubation process does not affect the crystal structure, however, and CuInSe₂ nanocrystals prepared either way are both cubic, as shown in Figure 3c and Figure 3d.

The CuInSe₂, CuIn_{0.6}Ga_{0.4}Se₂, and CuGaSe₂ nanocrystals made with long nucleation times of 12 h at 110 °C were all

cubic (fcc). Figure 2d shows the XRD patterns of the nanocrystals. As expected, the nanocrystals with higher amounts of Ga have smaller lattice constants. The optical gap also shifts to higher energy with increasing Ga, as shown in Figure 2e. The values of the optical gaps are consistent with bulk values. Elemental compositions determined by EDS are shown in Table 1. The In:Ga molar ratio of the CIGSe nanocrystals turns out to be slightly higher than the molar ratio of the reactants used to make them. When equimolar quantities of InCl₃ and GaCl₃ were added to the reaction, CIGSe nanocrystals were produced with an In:Ga ratio of 3:2. The lattice constant of 5.74 Å determined from the XRD data in Figure 2c for the CIGSe nanocrystals is also consistent with an In:Ga ratio of 3:2.

CulnSe₂, CuGaSe₂, and CIGSe Nanocrystal Synthesis in OLAm with DPP. The addition of DPP to the low temperature incubation step significantly increases the nucleation rate of the nanocrystals. The reaction mixture turns black almost immediately after DPP is added. The resulting nanocrystals are spherical, relatively uniform in size and contain Ga when added to the reaction. Figure 4 shows TEM, XRD, and UV-vis-NIR absorbance spectra for CuInSe₂, CuIn_{0.6}Ga_{0.4}Se₂, and CuGaSe nanocrystals synthesized in OLAm with DPP added during the low temperature nucleation step. The compositions of the nanocrystals made for this study are summarized in Table 1. Similar to the reactions without DPP, the CIGSe nanocrystals are slightly enriched with In compared to the reactant concentrations. CuIn_{0.6}Ga_{0.4}Se₂ nanocrystals were produced when equimolar ratios of In:Ga were used in the reaction. The optical gap also shifts to higher energy with increasing Ga concentrations as

One key difference in the nanocrystal product observed when DPP was added was that the $CuIn_{0.6}Ga_{0.4}Se_2$ and CuGaSe nanocrystals had wurtzite (hcp) crystal structure. The $CuInSe_2$ nanocrystals synthesized with DPP are still cubic.

			ve (1: 1 (C)			
			composition (normalized to Se)			
temp (°C)	solvent	nanocrystal	Cu	In	Ga	Se
240	OLAm	CuInSe ₂	0.96 ± 0.07	1.05 ± 0.09		2.0 ± 0.1
240	OLAm	$CuIn_{0.6}Ga_{0.4}Se_2$	0.94 ± 0.07	0.59 ± 0.09	0.43 ± 0.07	2.0 ± 0.4
280	OLAm	CuGaSe ₂	0.93 ± 0.07		1.04 ± 0.09	2.0 ± 0.1
240	OLAm + DPP	CuInSe ₂	0.92 ± 0.08	1.1 ± 0.1		2.0 ± 0.3
240	OLAm + DPP	$CuIn_{0.6}G_{a0.4}Se_2$	0.87 ± 0.03	0.62 ± 0.08	0.48 ± 0.09	2.0 ± 0.1
240	OLAm + DPP	CuGaSe ₂	1.03 ± 0.08		1.1 ± 0.2	2.0 ± 0.4
110	OLAm	CuInSe ₂	0.63 ± 0.05	1.2 ± 0.1		2.0 ± 0.3
110	OLAm + DPP	CuInSe ₂	0.70 ± 0.06	1.2 ± 0.1		2.0 ± 0.3
200	OLAm	CuGaSe ₂	0.76 ± 0.06		1.0 ± 0.2	2.0 ± 0.3
110	OLAm + DPP	CuGaSe ₂	1.06 ± 0.08		1.0 ± 0.2	2.0 ± 0.3

Table 1. Elemental Compositions Determined by EDS for CuIn, Ga1-xSe2 Nanocrystals Made in This Study

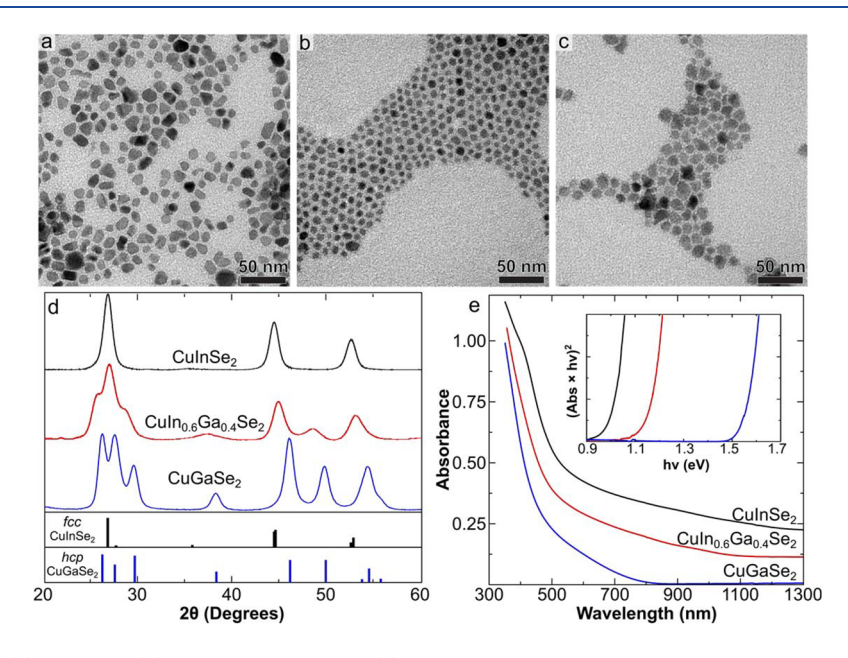


Figure 4. TEM images of (a) CuInSe₂, (b) CuIn_{0.6}Ga_{0.4}Se₂, and (c) CuGaSe₂ nanocrystals synthesized in OLAm with DPP added to the low temperature incubation step. (d) XRD of the CuInSe₂ (black), CuIn_{0.6}Ga_{0.4}Se₂ (red), and CuGaSe₂ (blue) nanocrystals. The XRD reference patterns displayed are for fcc CuInSe₂ (JCPDS no. 00-040-1487) and wurtzite (hcp) CuGaSe₂ calculated by the CaRIne Crystallography 3.1 program using space group P63mc (no. 186) and unit cell dimensions of a = b = 3.942 Å and c = 6.502 Å as in Pan et al.³¹ (e) Room temperature UV-vis-NIR absorbance spectra of the CuInSe₂ (black), CuIn_{0.6}Ga_{0.4}Se₂ (red), and CuGaSe₂ (blue) nanocrystals dispersed in toluene. The spectra are vertically offset for clarity. Inset: Plot of (Abs × $h\nu$)² vs $h\nu$ used to estimate optical gaps of the CuInSe₂, CuIn_{0.6}Ga_{0.4}Se₂, and CuGaSe₂ nanocrystals of 0.98 eV, 1.14 eV, and 1.61 eV, respectively.

Figure 4d shows a comparison of the XRD data for CuInSe₂, CuIn_{0.6}Ga_{0.4}Se₂, and CuGaSe₂ nanocrystals. DPP changes the crystal structure of CIGSe and CuGaSe₂ nanocrystals from fcc to hcp but does not affect the crystal structure of CuInSe₂. The hcp structure has little effect on the optical properties of the CIGSe nanocrystals. The spectra in Figure 4e are similar to the spectra for the fcc nanocrystals in Figure 2e, which is consistent with the fact that they have similar atomic configuration.³⁰

CuInSe₂ and CuGaSe₂ Nanocrystal Nucleation. The evolution of the CuInSe₂ and CuGaSe₂ nanocrystals during the low temperature nucleation step at 110 °C in OLAm (with and without DPP) was followed by isolating the reaction products after 30 min, 12 h, and 24 h and examining them by XRD, TEM, and UV-vis-NIR absorbance spectroscopy. Figure 5a-f shows the XRD data for the CuInSe₂ nanocrystals. There is a significant difference in the intermediate "seeds" when DPP is added. In pure OLAm, it takes more than 12 h for crystalline CuInSe₂ seed particles to form. As shown in Figure 5a-c, the

only crystalline materials present in the early stages of the low temperature incubation are hexagonal Se and CuSe. After 24 h, all of the materials have converted to fcc CuInSe2. When DPP is added, the nanocrystals exhibit crystalline fcc CuInSe2 structure after only 30 min. DPP greatly sped the formation of CuInSe₂ nanocrystals with cubic crystal structure. The TEM images and absorbance spectra were similar for the CuInSe₂ seed nanocrystals isolated after 24 h at 110 °C in OLAm made with or without DPP, as shown in Figure 5g-j. Both methods yield dispersible CuInSe₂ nanocrystals that are roughly 2-3 nm diameter with fcc crystal structure. The absorbance spectra (Figure 5i) of the CuInSe₂ seed nanocrystals isolated after 24 h at 110 °C exhibit broad exciton peaks and blue-shifted absorption edges compared to the nanocrystals obtained after the higher temperature growth step at 240 °C (Figure 4e). This is due to their smaller size and quantum confinement of their optical properties.¹⁵

Figure 6 shows similar data for CuGaSe₂ nanocrystals isolated at different stages of the low temperature incubation

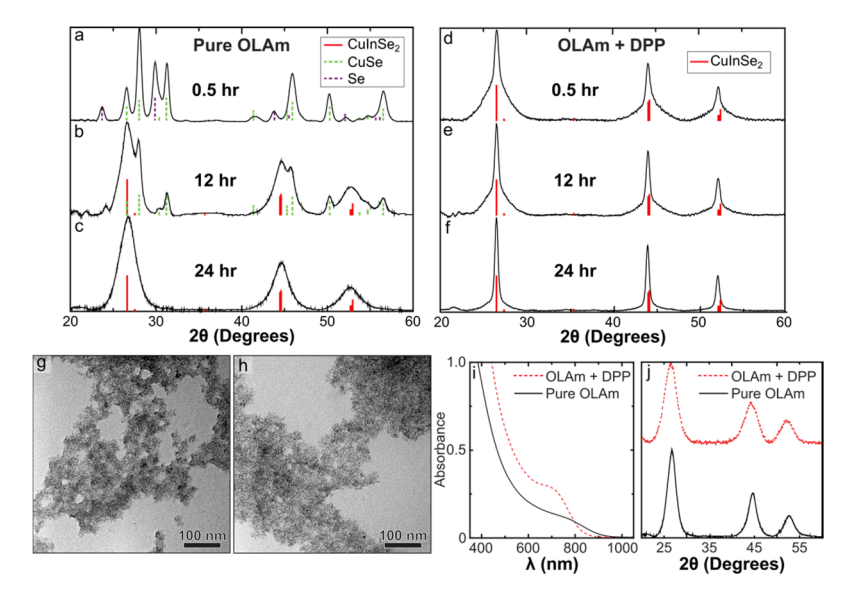


Figure 5. Powder XRD patterns of the crude product precipitated from the CuInSe₂ reaction. (a-c) The reaction proceeded in pure OLAm at 110 °C for (a) 0.5 h, (b) 12 h, and (c) 24 h. (d-f) The reaction proceeded at 110 °C in a mixture of OLAm and DPP (5.7% molar DPP) for (d) 0.5 h, (e) 12 h, and (f) 24 h. The solid red lines correspond to the diffraction pattern of fcc CuInSe₂ (JCPDS no. 00-040-1487). The dashed green lines correspond to hexagonal CuSe (PDF no. 00-006-0427), and the dashed purple lines are for hexagonal Se (PDF no. 00-006-0362). (g, h) TEM images of CuInSe₂ seed nanocrystals isolated from an incubation step in (g) pure OLAm or (h) 5.7 mol % DPP in OLAm. (i) UV-vis-NIR absorbance spectra and (j) XRD for the CuInSe₂ nanocrystals isolated after heating in OLAm with and without DPP at 110 °C for 24 h.

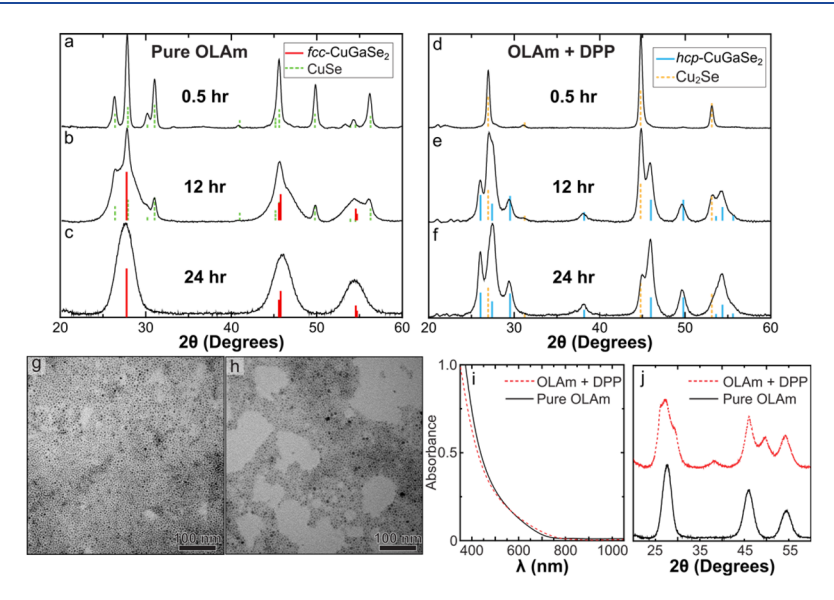


Figure 6. Powder XRD patterns of the crude product precipitated from the CuGaSe₂ reaction. (a–c) The reaction proceeded in pure OLAm at 200 °C for (a) 0.5 h, (b) 12 h, and (c) 24 h. (d–f) The reaction proceeded at 110 °C in a mixture of OLAm and DPP (5.7% molar DPP) for (d) 0.5 h, (e) 12 h, and (f) 24 h. The solid red lines correspond to the expected diffraction pattern for fcc CuGaSe₂ with a lattice parameter of 5.61 Å. Dashed green lines correspond to the expected pattern for hexagonal CuSe, PDF no. 00-006-0427. Dashed gold lines indicate the expected pattern for cubic Cu₂Se, PDF no. 00-006-0680. Solid blue lines indicate the simulated diffraction pattern for wurtzite (hcp) CuGaSe₂. The expected XRD pattern for hcp CuGaSe₂ was calculated using the CaRIne Crystallography 3.1 program using the space group P63mc (no. 186) and unit cell dimentions of a = b = 3.942 Å and c = 6.502 Å. (g, h) TEM images of the purified CuGaSe₂ seed nanocrystals synthesized in pure OLAm and in a mixture of 5.7 mol % DPP in OLAm, respectively. (i) UV-vis-NIR absorbance and (j) XRD for CuGaSe₂ seed nanocrystals isolated after 24 h from the low temperature nucleation step at 200 °C in OLAm and at 110 °C in OLAm with DPP.

step. The first thing to notice is that the nucleation of the CuGaSe₂ nanocrystals was much slower than the CuInSe₂ nanocrystals. In fact, the only crystalline product obtained from reactions with CuCl, GaCl₃, and Se in OLAm heated for 24 h at 110 °C was hexagonal CuSe (see Supporting Information). To obtain crystalline CuGaSe₂, it was necessary to raise the temperature of the incubation step to 200 °C. The nanocrystal

nucleation and growth rate was still very slow, but crystalline CuGaSe₂ product could be obtained after 24 h. Figure 6a–c shows XRD data for the reaction product isolated at different times. After 30 min, only hexagonal CuSe is present. After 12 h, there is a mixture of hexagonal CuSe and crystalline fcc CuGaSe₂. Finally, after 24 h, the residual product is crystalline fcc CuGaSe₂ nanocrystals.

Figure 6d–f shows XRD patterns of the material isolated when DPP was added to the reaction at lower temperature of 110 °C. The nucleation rate for CuGaSe₂ nanocrystals is significantly enhanced. Some crystalline CuGaSe₂ is observed after 12 h at 110 °C when DPP was added. After 30 min, only cubic Cu₂Se is observed. After 12 h, most of the product has converted to hcp CuGaSe₂, and after 24 h, it is all hcp CuGaSe₂. DPP significantly enhances the nucleation rate and reduces the temperature required to form crystalline CuGaSe₂ and also leads to the hcp phase.

The absorbance spectra of the hcp and fcc seed nanocrystals of CuGaSe₂ are compared in Figure 6i. The optical absorption of the seed nanocrystals is shifted to shorter wavelengths compared to the nanocrystals obtained after the higher temperature growth stage at 240 °C, indicating that there is some quantum confinement due to their small size. Figure 6g and Figure 6h show TEM images of the nanocrystals, which have diameters ranging between 3 and 5 nm. The spectra of the hcp and fcc CuGaSe₂ seed nanocrystals are similar and unaffected by their different crystal structures.

DISCUSSION

Long Nucleation Times in CIGSe Nanocrystal Reactions. Synthetic methods for CuInSe2 nanocrystals fall into two categories: heat-up and hot injection.²⁰ The heat-up method of Panthani et al.²⁴ for example involves the reaction between metal chlorides and Se powder in OLAm to produce CuInSe₂ and CuIn_xGa_{1-x}Se₂ nanocrystals with equilibrium fcc structure. The initial "degassing" step reported in ref 22 in which the reaction is held at 110 °C under vacuum for an extended period of time turns out to be crucial for generating approximately spherical, dispersible nanocrystals. As described above, this low temperature step provides enough time for nucleation to occur, and without it (when the nucleation step is cut short) CuInSe₂ nanocrystals are generated with a flower or sheet-like morphology and very low reaction yields (<10% conversion). In the case of CIGSe nanocrystals, this long lowtemperature incubation period is even more important. Without it, no Ga incorporates into the nanocrystals.

Hot-injection schemes offer faster nucleation and growth and much shorter process times to generate nanocrystals. We have been especially interested in reactions involving phosphine-Se complexes like DPP-Se, because it has been shown to provide the highest yields of dispersible CuInSe₂ nanocrystals and printed PV devices with the highest efficiencies from these materials. 15,32 Hot-injection DPP-Se reactions had not previously been explored for CuGaSe2 and CIGSe nanocrystals. The fast nucleation induced by DPP reported here also enables the hot injection synthesis of CIGSe and CuGaSe₂ nanocrystals but with hcp structure. Under similar reaction conditions, CuInSe2 nanocrystals are produced with fcc structure. As illustrated in Figure 7, the only difference between the two structures is the ABCABC and ABABAB stacking of close-packed planes.³³ When the nucleation rate is fast, this induces formation of the hcp phases of CuGaSe₂ and CIGSe nanocrystals. The subtle differences between the calculated and experimental diffraction peak intensities in Figure 4d for the CuGaSe₂ and CuIn_{0.6}Ga_{0.4}Se₂ nanocrystals indicate that stacking faults are present, giving rise to some mixed fcc-hcp character.

The formation of the hcp phase has been observed in nanocrystals of related materials, $\text{CuIn}_x\text{Ga}_{x-1}\text{S}_2$, $^{31,34-39}$ CuInSe_2 , 19,22,23,40 Cu_2SnSe , 41 and $\text{Cu}_2\text{ZnSnS}_4$. Tappan et

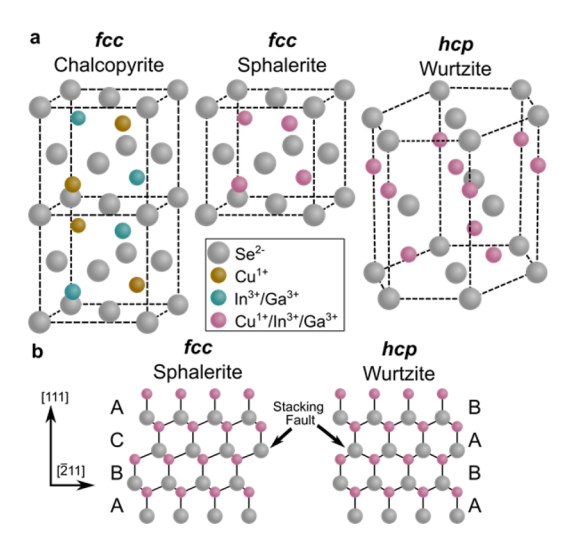


Figure 7. (a) Illustration of the chalcopyrite, sphalerite, and wurtzite $CuIn_xGa_{1-x}Se_2$ crystal structures drawn with an Se atom in the (0,0,0) site. The chalcopyrite and sphalerite structures consist of cations arranged around an fcc Se lattice, while the wurtzite structure consists of the cations arranged around an hcp Se lattice. (b) Illustration of the sphalerite structure viewed along $[01\overline{1}]$ and the stacking faults that lead to the wurtzite structure.

al. 19 showed that fast nucleation in the case of CuInSe₂ nanocrystals leads to fcc crystal structure, which is consistent with our observations as well. But when Ga is present, faster nucleation leads to the hcp phase for CuGaSe₂ and CIGSe nanocrystals.

CONCLUSIONS

The addition of Ga to CuInSe2 nanocrystal syntheses significantly alters the nanocrystal growth kinetics. The rate of nucleation and growth of CuInSe₂ nanocrystals in OLAm is extremely slow, and the presence of Ga makes it even slower. A long incubation period at low temperature is needed to obtain spherical nanocrystals with reasonable product yields. Under these conditions CuInSe2, CuGaSe2, and CIGSe nanocrystals all exhibit fcc crystal structure. The addition of DPP significantly enhances the nucleation rates. It does not change the crystal structure of CuInSe₂ nanocrystals, but the much faster nucleation rates lead to hcp crystal structure for the CuGaSe₂ and CIGSe nanocrystals. This is the first report of CuGaSe, and CIGSe nanocrystals exhibiting the hcp phase. The optical properties of the nanocrystals are unaffected by the difference in crystal structure, and most likely high temperature selenization of these nanocrystals into polycrystalline films converts them to the equilibrium chalcopyrite phase anyway, but it is important to recognize the effect of Ga on the nanocrystal growth kinetics in order to generate materials with controlled stoichiometry and reliable yield. Ga is known to provide synthetic challenges in other cases as well, like GaAs. 44-46 Perhaps DPP has a role to play there too.

ASSOCIATED CONTENT

S Supporting Information

The Supporting Information is available free of charge on the ACS Publications website at DOI: 10.1021/acsanm.9b01237.

XRD of reaction products isolated from a $CuGaSe_2$ nanocrystal reaction in OLAm at 110 °C after 24 h (PDF)

AUTHOR INFORMATION

Corresponding Author

*E-mail: korgel@che.utexas.edu. Phone: +1-512-471-5633.

ORCID ®

Timothy D. Siegler: 0000-0001-6033-2232 Brian A. Korgel: 0000-0001-6242-7526

Notes

The authors declare no competing financial interest.

ACKNOWLEDGMENTS

Financial support for this work is acknowledged from the Robert A. Welch Foundation (Grant F-1464) and the NSF Industry/University Cooperative Research Center on Next Generation Photovoltaics (Grants IIP-1540028 and IIP-1822206). T.D.S. acknowledges United States government support under an award by DoD, Air Force Office of Scientific Research, National Defense Science and Engineering Graduate (NDSEG) Fellowship, 32 CFR 168a.

REFERENCES

- (1) Chen, B.; Pradhan, N.; Zhong, H. From Large-Scale Synthesis to Lighting Device Applications of Ternary I—III—VI Semiconductor Nanocrystals: Inspiring Greener Material Emitters. *J. Phys. Chem. Lett.* **2018**, *9*, 435–445.
- (2) Panthani, M. G.; Khan, T. A.; Reid, D. K.; Hellebusch, D. J.; Rasch, M. R.; Maynard, J. A.; Korgel, B. A. In Vivo Whole Animal Fluorescence Imaging of a Microparticle-Based Oral Vaccine Containing (CuInSe_xS_{2x})/ZnS Core/Shell Quantum Dots. *Nano Lett.* 2013, 13, 4294–4298.
- (3) Meinardi, F.; McDaniel, H.; Carulli, F.; Colombo, A.; Velizhanin, K. A.; Makarov, N. S.; Simonutti, R.; Klimov, V. I.; Brovelli, S. Highly Efficient Large-Area Colourless Luminescent Solar Concentrators Using Heavy-Metal-Free Colloidal Quantum Dots. *Nat. Nanotechnol.* **2015**, *10*, 878–885.
- (4) Cassette, E.; Pons, T.; Bouet, C.; Helle, M.; Bezdetnaya, L.; Marchal, F.; Dubertret, B. Synthesis and Characterization of Near-Infrared Cu–In–Se/ZnS Core/Shell Quantum Dots for In Vivo Imaging. *Chem. Mater.* **2010**, 22, 6117–6124.
- (5) Li, J.; Jin, H.; Wang, K.; Xie, D.; Xu, D.; Xu, X.; Xu, G. High Luminance of CuInS₂ -Based Yellow Quantum Dot Light Emitting Diodes Fabricated by All-Solution Processing. *RSC Adv.* **2016**, *6*, 72462–72470.
- (6) Pernik, D. R.; Gutierrez, M.; Thomas, C.; Voggu, V. R.; Yu, Y.; van Embden, J.; Topping, A. J.; Jasieniak, J. J.; Vanden Bout, D. A.; Lewandowski, R.; Korgel, B. A. Plastic Microgroove Solar Cells Using CuInSe₂ Nanocrystals. *ACS Energy Lett.* **2016**, *1*, 1021–1027.
- (7) Voggu, V. R.; Sham, J.; Pfeffer, S.; Pate, J.; Fillip, L.; Harvey, T. B.; Brown, R. M.; Korgel, B. A. Flexible CuInSe₂ Nanocrystal Solar Cells on Paper. *ACS Energy Lett.* **2017**, *2*, 574–581.
- (8) Chirila, A.; Reinhard, P.; Pianezzi, F.; Bloesch, P.; Uhl, A. R.; Fella, C.; Kranz, L.; Keller, D.; Gretener, C.; Hagendorfer, H.; Jaeger, D.; Erni, R.; Nishiwaki, S.; Buecheler, S.; Tiwari, A. N. Potassium-Induced Surface Modification of Cu(In,Ga)Se₂ Thin Films for High Efficiency Solar Cells. *Nat. Mater.* **2013**, *12*, 1107–1111.
- (9) Carron, R.; Nishiwaki, S.; Feurer, T.; Hertwig, R.; Avancini, E.; Löckinger, J.; Yang, S.-C.; Buecheler, S.; Tiwari, A. N. Advanced Alkali Treatments for High-Efficiency Cu(In,Ga)Se₂ Solar Cells on Flexible Substrates. *Adv. Energy Mater.* **2019**, *9*, 1900408.
- (10) Guo, Q.; Ford, G. M.; Hillhouse, H. W.; Agrawal, R. Sulfide Nanocrystal Inks for Dense Cu(In_{1-x}Ga_x)(S_{1-y}Se_y)₂ Absorber Films and Their Photovoltaic Performance. *Nano Lett.* **2009**, *9*, 3060–3065.
- (11) Guo, Q.; Ford, G. M.; Agrawal, R.; Hillhouse, H. W. Ink Formulation and Low-Temperature Incorporation of Sodium to Yield 12% Efficient Cu(In,Ga)(S,Se)₂ Solar Cells from Sulfide Nanocrystal Inks. *Prog. Photovoltaics* **2013**, *21*, 64–71.

- (12) Harvey, T. B.; Mori, I.; Stolle, C. J.; Bogart, T. D.; Ostrowski, D. P.; Glaz, M. S.; Du, J.; Pernik, D. R.; Akhavan, V. A.; Kesrouani, H.; Vanden Bout, D. A.; Korgel, B. A. Copper Indium Gallium Selenide (CIGS) Photovoltaic Devices Made Using Multistep Selenization of Nanocrystal Films. ACS Appl. Mater. Interfaces 2013, 5, 9134–9140.
- (13) Houck, D. W.; Siegler, T.; Korgel, B. A. Predictive Modeling of CuInSe₂ Nanocrystal Photovoltaics: The Importance of Band Alignment and Carrier Diffusion. *ACS Appl. Energy Mater.* **2019**, *2*, 1494–1504.
- (14) Allen, P. M.; Bawendi, M. G. Ternary I-III-VI Quantum Dots Luminescent in the Red to Near-Infrared. J. Am. Chem. Soc. 2008, 130, 9240-9241.
- (15) Panthani, M. G.; Stolle, C. J.; Reid, D. K.; Rhee, D. J.; Harvey, T. B.; Akhavan, V. A.; Yu, Y.; Korgel, B. A. CuInSe₂ Quantum Dot Solar Cells with High Open-Circuit Voltage. *J. Phys. Chem. Lett.* **2013**, 4, 2030–2034.
- (16) Yarema, O.; Yarema, M.; Wood, V. Tuning the Composition of Multicomponent Semiconductor Nanocrystals: The Case of I–III–VI Materials. *Chem. Mater.* **2018**, *30*, 1446–1461.
- (17) Houck, D. W.; Korgel, B. A. Facile Exchange of Tightly Bonded L-Type Oleylamine and Diphenylphosphine Ligands on Copper Indium Diselenide Nanocrystals Mediated by Molecular Iodine. *Chem. Mater.* **2018**, *30*, 8359–8367.
- (18) Houck, D. W.; Assaf, E. I.; Shin, H.; Greene, R. M.; Pernik, D. R.; Korgel, B. A. Pervasive Cation Vacancies and Anti-Site Defects in Copper Indium Diselenide (CuInSe₂) Nanocrystals. *J. Phys. Chem. C* **2019**, 123, 9544–9551.
- (19) Tappan, B. A.; Barim, G.; Kwok, J. C.; Brutchey, R. L. Utilizing Diselenide Precursors toward Rationally Controlled Synthesis of Metastable CuInSe₂ Nanocrystals. *Chem. Mater.* **2018**, *30*, 5704–5713.
- (20) Coughlan, C.; Ibáñez, M.; Dobrozhan, O.; Singh, A.; Cabot, A.; Ryan, K. M. Compound Copper Chalcogenide Nanocrystals. *Chem. Rev.* 2017, 117 (9), 5865–6109.
- (21) Kar, M.; Agrawal, R.; Hillhouse, H. W. Formation Pathway of CuInSe₂ Nanocrystals for Solar Cells. *J. Am. Chem. Soc.* **2011**, *133*, 17239–17247.
- (22) Wang, J.-J.; Wang, Y.-Q.; Cao, F.-F.; Guo, Y.-G.; Wan, L.-J. Synthesis of Monodispersed Wurtzite Structure CuInSe₂ Nanocrystals and Their Application in High-Performance Organic—Inorganic Hybrid Photodetectors. *J. Am. Chem. Soc.* **2010**, *132*, 12218–12221.
- (23) Norako, M. E.; Brutchey, R. L. Synthesis of Metastable Wurtzite CuInSe₂ Nanocrystals. *Chem. Mater.* **2010**, 22, 1613–1615. (24) Panthani, M. G.; Akhavan, V.; Goodfellow, B.; Schmidtke, J. P.; Dunn, L.; Dodabalapur, A.; Barbara, P. F.; Korgel, B. A. Synthesis of CuInS₂, CuInSe₂, and Cu(In_xGa_{1-x})Se₂ (CIGS) Nanocrystal "Inks" for Printable Photovoltaics. *J. Am. Chem. Soc.* **2008**, 130, 16770–
- (25) Ahmadi, M.; Pramana, S. S.; Xi, L.; Boothroyd, C.; Lam, Y. M.; Mhaisalkar, S. Evolution Pathway of CIGSe Nanocrystals for Solar Cell Applications. *J. Phys. Chem. C* **2012**, *116*, 8202–8209.
- (26) Evans, C. M.; Evans, M. E.; Krauss, T. D. Mysteries of TOPSe Revealed: Insights into Quantum Dot Nucleation. *J. Am. Chem. Soc.* **2010**, *132*, 10973–10975.
- (27) Qi, T.; Yang, H.-Q.; Whitfield, D. M.; Yu, K.; Hu, C.-W. Insights into the Mechanistic Role of Diphenylphosphine Selenide, Diphenylphosphine, and Primary Amines in the Formation of CdSe Monomers. *J. Phys. Chem. A* **2016**, *120*, 918–931.
- (28) Steckel, J. S.; Yen, B. K. H.; Oertel, D. C.; Bawendi, M. G. On the Mechanism of Lead Chalcogenide Nanocrystal Formation. *J. Am. Chem. Soc.* **2006**, *128*, 13032–13033.
- (29) Joo, J.; Pietryga, J. M.; McGuire, J. A.; Jeon, S.-H.; Williams, D. J.; Wang, H.-L.; Klimov, V. I. A Reduction Pathway in the Synthesis of PbSe Nanocrystal Quantum Dots. *J. Am. Chem. Soc.* **2009**, *131*, 10620–10628.
- (30) Stanbery, B. J. Copper Indium Selenides and Related Materials for Photovoltaic Devices. *Crit. Rev. Solid State Mater. Sci.* **2002**, *27*, 73–117.

- (31) Pan, D.; An, L.; Sun, Z.; Hou, W.; Yang, Y.; Yang, Z.; Lu, Y. Synthesis of Cu–In–S Ternary Nanocrystals with Tunable Structure and Composition. *J. Am. Chem. Soc.* **2008**, *130*, 5620–5621.
- (32) Akhavan, V. A.; Panthani, M. G.; Goodfellow, B. W.; Reid, D. K.; Korgel, B. A. Thickness-Limited Performance of CuInSe₂ Nanocrystal Photovoltaic Devices. *Opt. Express* **2010**, *18*, A411.
- (33) Yeh, C.-Y.; Lu, Z. W.; Froyen, S.; Zunger, A. Zinc-Blende-Wurtzite Polytypism in Semiconductors. *Phys. Rev. B: Condens. Matter Mater. Phys.* **1992**, *46*, 10086.
- (34) Koo, B.; Patel, R. N.; Korgel, B. A. Wurtzite-Chalcopyrite Polytypism in CuInS, Nanodisks. *Chem. Mater.* **2009**, *21*, 1962–1966.
- (35) Batabyal, S. K.; Tian, L.; Venkatram, N.; Ji, W.; Vittal, J. J. Phase-Selective Synthesis of CuInS₂ Nanocrystals. *J. Phys. Chem. C* **2009**, *113*, 15037–15042.
- (36) Kruszynska, M.; Borchert, H.; Parisi, J.; Kolny-Olesiak, J. Synthesis and Shape Control of CuInS₂ Nanoparticles. *J. Am. Chem. Soc.* **2010**, *132*, 15976–15986.
- (37) Nose, K.; Soma, Y.; Omata, T.; Otsuka-Yao-Matsuo, S. Synthesis of Ternary CuInS₂ Nanocrystals; Phase Determination by Complex Ligand Species. *Chem. Mater.* **2009**, *21*, 2607–2613.
- (38) Lu, X.; Zhuang, Z.; Peng, Q.; Li, Y. Controlled Synthesis of Wurtzite CuInS₂ Nanocrystals and Their Side-by-Side Nanorod Assemblies. *CrystEngComm* **2011**, *13*, 4039–4045.
- (39) Wang, Y.-H. A.; Zhang, X.; Bao, N.; Lin, B.; Gupta, A. Synthesis of Shape-Controlled Monodisperse Wurtzite CuIn_xGa_{1-x}S₂ Semiconductor Nanocrystals with Tunable Band Gap. *J. Am. Chem. Soc.* **2011**, *133*, 11072–11075.
- (40) Sousa, V.; Goncalves, B. F.; Franco, M.; Ziouani, Y.; Gonzalez-Ballesteros, B.; Cerqueira, M. F.; Yannello, V.; Kovnir, K.; Lebedev, O. I.; Kolen'ko, Y. V. Superstructural Ordering in Hexagonal CuInSe₂ Nanoparticles. *Chem. Mater.* **2019**, *31*, 260–267.
- (41) Norako, M. E.; Greaney, M. J.; Brutchey, R. L. Synthesis and Characterization of Wurtzite-Phase Copper Tin Selenide Nanocrystals. *J. Am. Chem. Soc.* **2012**, *134*, 23–26.
- (42) Lu, X.; Zhuang, Z.; Peng, Q.; Li, Y. Wurtzite Cu₂ZnSnS₄ Nanocrystals: A Novel Quaternary Semiconductor. *Chem. Commun.* **2011**, *47*, 3141–3143.
- (43) Singh, A.; Geaney, H.; Laffir, F.; Ryan, K. M. Colloidal Synthesis of Wurtzite Cu₂ZnSnS₄ Nanorods and Their Perpendicular Assembly. *J. Am. Chem. Soc.* **2012**, *134*, 2910–2913.
- (44) Srivastava, V.; Liu, W.; Janke, E. M.; Kamysbayev, V.; Filatov, A. S.; Sun, C.-J.; Lee, B.; Rajh, T.; Schaller, R. D.; Talapin, D. V. Understanding and Curing Structural Defects in Colloidal GaAs Nanocrystals. *Nano Lett.* 2017, 17, 2094–2101.
- (45) Davidson, F. M.; Schricker, A. D.; Wiacek, R. J.; Korgel, B. A. Supercritical Fluid-Liquid-Solid Synthesis of Gallium Arsenide Nanowires Seeded by Alkanethiol-Stabilized Gold Nanocrystals. *Adv. Mater.* **2004**, *16*, 646–649.
- (46) Dong, A.; Yu, H.; Wang, F.; Buhro, W. E. Colloidal GaAs Quantum Wires: Solution-Liquid-Solid Synthesis and Quantum-Confinement Studies. *J. Am. Chem. Soc.* **2008**, *130*, 5954–5961.